

https://doi.org/10.1070/QEL17496

Generation of few-cycle radiation pulses in the IR spectral range (1.3–2.2 μm) using wide-aperture BBO crystals pumped by a terawatt Ti:sapphire laser*

E.A. Migal, D.Z. Suleimanova, F.V. Potemkin

Abstract. **Different schemes of parametric amplification (PA), aimed at designing a source of femtosecond near-IR (1.3–2.2 μm) radiation, are compared by solving a system of truncated equations describing three-wave mixing. A terawatt Ti:sapphire laser with an energy of 60 mJ and a pulse duration of 50 fs is used as a pump source for PA schemes. The dependences of the output energies, pulse durations, and spectral widths of signal and idler waves on the BBO crystal length for two types of phase matching and on the group-delay dispersions for the pump and signal waves is investigated. It is shown that in the case of direct PA, using a type-II phase-matching BBO crystal of optimal length, one can obtain signal (1.333 μm) and idler (2 μm) waves with pulse durations of 34 and 32 fs, respectively, with a total energy conversion efficiency up to 40%. The application of double chirping scheme increases the total conversion efficiency to 60%; however, the spectral width of generated pulses decreases. The spectral width can only be increased by reducing the conversion efficiency. In this case, a more simple and compact solution is the scheme of direct PA with a transform-limited pump pulse.**

Keywords: *optical parametric amplifier, double chirping, mid-IR range, BBO crystal.*

1. Introduction

Intense few-cycle THz pulses are of great interest in view of the development of nonlinear THz photonics, which opens new possibilities for studying the strongly nonequilibrium dynamics of electron and phonon subsystems, ultrafast magnetisation, visualisation, etc. Efficient generation of THz radiation with a field strength up to several units of GV m^{-1} under optical pumping [1] became possible only recently, when organic crystals were developed [2]. These crystals (for example, DAST, DSTMS, and OH1) provide high nonlinearity and are transparent both for optical pumping and for THz radiation, due to which optical rectification is efficient. However, the dispersion properties of these materials call for a near-IR (1.2–1.5 μm) pump source. In addition, the efficiency of plasma THz sources has also been significantly increased recently due to the use of near- and mid-IR sources. The optimal pump wavelength for THz sources based on two-colour filamentation was predicted theoretically; it amounts to ~3.2 μm [3].

Unfortunately, to date there is only a limited number of laser media that can provide high-power (several tens of mJ) femtosecond (less than 100 fs) pump radiation in the near- and mid-IR ranges [4, 5]. In this context, the problem of developing efficient parametric sources pumped by available laser systems, based, for example, on Ti:sapphire crystals, remains urgent. This approach is one of the most promising, primarily due to the possibility of scaling the output energy of Ti:sapphire lasers with conservation of pulse duration at a level of 20–50 fs, which cannot be done in ytterbium systems because of the pronounced effects of gain band narrowing. Currently, an output power as high as several tens of petawatt has been attained for Ti:sapphire laser systems [6].

Due to the existence of high-power laser systems, new approaches to the design of parametric amplifiers are being developed. The research in this field is primarily motivated by the difficulties in using multimillijoule and terawatt radiation to pump parametric amplifiers. Here, important limitations are the self-action and cross effects, occurring when high-power radiation propagates in nonlinear media, as well as technological limitations on the growth of wide-aperture nonlinear optical crystals (necessary elements for the output cascades of parametric conversion). In this context, it has recently been proposed to use double chirping to design efficient terawatt parametric amplifiers (double chirped optical parametric amplifiers) [7]; this approach allows one to avoid undesirable nonlinear effects due to the chirping of both pump and signal waves. This scheme was successfully applied to generate 1.7-μm laser pulses with an energy of 0.1 J and a duration of 31 fs using a Ti:sapphire laser (0.77 J, 25 fs) as a pump source [8].

The efficiency of double chirping stimulates researchers to search for and choose a specific approach to the design of a high-power parametric amplifier. The purpose of this study was to perform a theoretical comparison of direct amplification schemes using spectrally limited and chirped

*Presented at the 4th International Conference on Ultrafast Optical Science (Russia, Moscow, FIAN, 28 September – 2 October 2020).

E.A. Migal, D.Z. Suleimanova, F.V. Potemkin Faculty of Physics, Lomonosov Moscow State University, Vorob'evy gory, 119991 Moscow, Russia;
e-mail: ea.migalj@physics.msu.ru

Received 30 November 2020; revision received 26 April 2021
Kvantovaya Elektronika **51** (7) 601–608 (2021)
Translated by Yu.P. Sin'kov

pulses for conversion into the near-IR range (1.333–2.2 μm). A terawatt Ti:sapphire laser with a pulse energy of 60 mJ and a pulse duration of 50 fs was used as pump source (there is a laser with such characteristics at Lomonosov Moscow State University).

2. Numerical model description

To determine the efficiency of conversion into signal and idler waves and estimate the spectral width of signal and idler pulses in different schemes of parametric amplification (PA), we performed a numerical simulation based on solving a system of truncated equations describing the three-wave interaction.

The PA was considered in the approximations of slowly varying amplitudes and plane waves in the second approximation of dispersion theory. The model in use takes into account the second-order nonlinear processes responsible for the PA and second-harmonic generation, as well as the third-order processes: self-phase modulation and cross modulation. In this case, the PA is described by the system of truncated equations

$$\frac{\mathrm{d}A_\mathrm{s}}{\mathrm{d}z}+\beta_{1\mathrm{s}}\frac{\partial A_\mathrm{s}}{\partial t}+\mathrm{i}\frac{\beta_{2\mathrm{s}}}{2}\frac{\partial^2 A_\mathrm{s}}{\partial t^2}=-\mathrm{i}\frac{\omega_\mathrm{s}}{c}$$

$$\times\left[\left(\frac{d_\mathrm{eff}}{n_\mathrm{s}}A_\mathrm{p}A_\mathrm{i}^*+n_{2\mathrm{s}}^\mathrm{s}|A_\mathrm{s}|^2A_\mathrm{s}\right.\right.$$

$$\left.+2n_{2\mathrm{s}}^\mathrm{x}|A_\mathrm{i}|^2A_\mathrm{s}+2n_{2\mathrm{s}}^\mathrm{x}|A_\mathrm{p}|^2A_\mathrm{s}\right)$$

$$\left.\times\exp(-\mathrm{i}\Delta kz)+\frac{d_{\mathrm{eff\,s\,SH}}A_\mathrm{s}^*A_{\mathrm{s\,SH}}}{n_\mathrm{s}}\exp(-\mathrm{i}\Delta k_{\mathrm{s\,SH}}z)\right],$$

$$\frac{\mathrm{d}A_\mathrm{i}}{\mathrm{d}z}+\beta_{1\mathrm{i}}\frac{\partial A_\mathrm{i}}{\partial t}+\mathrm{i}\frac{\beta_{2\mathrm{i}}}{2}\frac{\partial^2 A_\mathrm{i}}{\partial t^2}=-\mathrm{i}\frac{\omega_\mathrm{i}}{c}$$

$$\times\left[\left(\frac{d_\mathrm{eff}}{n_\mathrm{i}}A_\mathrm{p}A_\mathrm{s}^*+n_{2\mathrm{i}}^\mathrm{s}|A_\mathrm{i}|^2A_\mathrm{i}\right.\right.$$

$$\left.+2n_{2\mathrm{i}}^\mathrm{x}|A_\mathrm{s}|^2A_\mathrm{i}+2n_{2\mathrm{i}}^\mathrm{x}|A_\mathrm{p}|^2A_\mathrm{i}\right)$$

$$\left.\times\exp(-\mathrm{i}\Delta kz)+\frac{d_{\mathrm{eff\,i\,SH}}A_\mathrm{i}^*A_{\mathrm{i\,SH}}}{n_\mathrm{i}}\exp(-\mathrm{i}\Delta k_{\mathrm{i\,SH}}z)\right], \quad (1)$$

$$\frac{\mathrm{d}A_\mathrm{p}}{\mathrm{d}z}+\beta_{1\mathrm{p}}\frac{\partial A_\mathrm{p}}{\partial t}+\mathrm{i}\frac{\beta_{2\mathrm{p}}}{2}\frac{\partial^2 A_\mathrm{p}}{\partial t^2}=-\mathrm{i}\frac{\omega_\mathrm{p}}{c}$$

$$\times\left(\frac{d_\mathrm{eff}}{n_\mathrm{p}}A_\mathrm{s}A_\mathrm{i}+n_{2\mathrm{p}}^\mathrm{s}|A_\mathrm{s}|^2A_\mathrm{p}+2n_{2\mathrm{p}}^\mathrm{x}|A_\mathrm{i}|^2A_\mathrm{p}\right.$$

$$\left.+2n_{2\mathrm{p}}^\mathrm{x}|A_\mathrm{p}|^2A_\mathrm{p}\right)\exp(\mathrm{i}\Delta kz),$$

$$\frac{\mathrm{d}A_{\mathrm{s\,SH}}}{\mathrm{d}z}+\beta_{1\mathrm{s\,SH}}\frac{\partial A_{\mathrm{s\,SH}}}{\partial t}+\mathrm{i}\frac{\beta_{2\mathrm{s\,SH}}}{2}\frac{\partial^2 A_{\mathrm{s\,SH}}}{\partial t^2}=$$

$$=-\mathrm{i}\frac{\omega_{\mathrm{s\,SH}}}{c}\frac{d_{\mathrm{eff\,s\,SH}}}{n_{\mathrm{s\,SH}}}A_\mathrm{s}A_\mathrm{s}\exp(-\mathrm{i}\Delta k_{\mathrm{s\,SH}}z),$$

$$\frac{\mathrm{d}A_{\mathrm{i\,SH}}}{\mathrm{d}z}+\beta_{1\mathrm{i\,SH}}\frac{\partial A_{\mathrm{i\,SH}}}{\partial t}+\mathrm{i}\frac{\beta_{2\mathrm{i\,SH}}}{2}\frac{\partial^2 A_{\mathrm{i\,SH}}}{\partial t^2}$$

$$=-\mathrm{i}\frac{\omega_{\mathrm{i\,SH}}}{c}\frac{d_{\mathrm{eff\,i\,SH}}}{n_{\mathrm{i\,SH}}}A_\mathrm{i}A_\mathrm{i}\exp(-\mathrm{i}\Delta k_{\mathrm{i\,SH}}z),$$

where the subscripts s, i, and p correspond to signal, idler, and pump waves, respectively; SH stands for the second harmonic; $A_{\mathrm{s,i,p}}$ are the interacting-wave amplitudes; $\beta_1 = \mathrm{d}k/\mathrm{d}\omega = 1/v_\mathrm{g}$ is the first-order dispersion coefficient, equal to the inverse group velocity; $\beta_2 = \mathrm{d}^2k/\mathrm{d}\omega^2$ is the second-order dispersion coefficient, which determines the change in the pulse duration due to the group-velocity dispersion; d_eff is the effective nonlinearity coefficient; $\omega_{\mathrm{s,i,p}}$ are the interacting-wave frequencies; $n_{\mathrm{s,i,p}}$ are the refractive indices; n_2^s and n_2^x are the nonlinear refractive indices, determining the self-phase modulation and cross-modulation processes; c is the speed of light in vacuum; and Δk is the wave mismatch.

The equations were solved numerically by the finite-element method. The sweep method was applied after approximating the equations of system (1) by a system of algebraic equations with a tridiagonal matrix.

When simulating the direct PA scheme, a Gaussian pulse is applied at the crystal input and the following initial and boundary conditions are fulfilled:

$$E_m(z,t)=\frac{1}{2}E_{0m}\exp\left[-2\ln 2\left(\frac{t}{\Delta t_m}\right)^2\right]\exp(\mathrm{i}\omega_m t)+\mathrm{c.c.},$$

$$E_m\left(t=-\frac{T}{2}\right)=0,\quad E_m\left(t=\frac{T}{2}\right)=0, \quad (2)$$

where the subscript m = s, i, p; Δt_m is the pulse duration; and T is the time window width.

We also considered PA with chirped pump and signal waves. The phase can be written as

$$\Phi(t)=\Phi_0+\omega_0 t+\Phi_\mathrm{a}(t), \quad (3)$$

where Φ_0 is the absolute phase and $\Phi_\mathrm{a}(t)$ is time-dependent phase additive. The instantaneous frequency can be calculated from the formula

$$\omega(t)=\frac{\mathrm{d}\Phi(t)}{\mathrm{d}t}=\omega_0+\frac{\mathrm{d}\Phi_\mathrm{a}(t)}{\mathrm{d}t}. \quad (4)$$

Thus, the time-dependent phase additive describes the frequency variation with time (chirp). At $\Phi_\mathrm{a}(t) = \pm at^2$ the frequency changes linearly.

In the spectral representation the phase can be expanded in a Taylor series near the frequency ω_0:

$$\varphi(\omega)=\varphi(\omega_0)+\varphi'(\omega_0)(\omega-\omega_0)$$

$$+\frac{1}{2}\varphi''(\omega_0)(\omega-\omega_0)^2+\frac{1}{6}\varphi'''(\omega_0)(\omega-\omega_0)^3+\ldots \quad (5)$$

The first term in the expansion is related to the absolute phase: $\varphi(\omega_0) = -\Phi_0$. It follows from the Fourier transform properties that the second term is responsible for the shift of laser pulse envelope in the time representation. The higher order coefficients describe the changes in the temporal structure of field. For example, the presence of a nonzero coefficient $\varphi''(\omega_0)$ [also referred to as the group-delay dispersion (GDD)] corresponds to a linearly chirped pulse. The quadratic phase (linear chirp) was introduced to elongate the signal and pump pulses. Thus, the Gaussian pulse at the crystal input in the time representation had the form

$$E(t) = \frac{E_0}{2\gamma^{1/4}}\exp\left(-\frac{t^2}{4\beta\gamma}\right)\exp(\mathrm{i}\omega_0 t)\exp[\mathrm{i}(at^2 - \varepsilon)], \qquad (6)$$

where

$$\beta = \frac{\Delta t^2}{8\ln 2};\ \gamma = 1 + \frac{\varphi''^2}{4\beta^2};$$

$$a = \frac{\varphi''}{8\beta^2\gamma};\ \varepsilon = \frac{1}{2}\arctan\left(\frac{\varphi''}{2\beta}\right);$$

Δt is the initial duration of a transform-limited pulse.

The pump source was a terawatt Ti : sapphire laser (λ_p = 0.8 μm, W = 60 mJ). The pump pulse duration τ was 50 fs. In further calculations the pump intensity at the crystal input was 200 GW cm^{-2}, a value lower than the crystal breakdown threshold [9, 10]. This intensity value is also ultimate from the point of view of undesirable nonlinear effects, because the B integral at this pulse duration and a crystal length of 2 mm (which is an optimal value; see below) is estimated to be 0.9. It was noted in many studies that the value of the B integral should be below unity (see, e.g., [11]). A Ti:sapphire laser energy equal to 1 mJ was used in the simulation of the first PA cascade. Table 1 contains the pump and signal wave parameters accepted in the calculations.

To implement PA in the near-IR range (λ_s = 1.333 μm, λ_i = 2 μm), we chose a beta-barium borate crystal (β-BaB_2O_4, BBO), which has a wide transparency range (0.19–2.6 μm), a fairly large nonlinear optical coefficient, a large phase-matching spectral width, and a high breakdown threshold. The main crystal characteristics used in the simulation are listed in Table 2. The refractive index for each wave was calculated based on the Sellmeier formulae [12]. The value of nonlinear refractive index n_2 was taken from [13].

Table 1. Pump and signal wave parameters used in the simulation.

Radiation	Wavelength/μm	Initial energy	Initial pulse duration/fs
Pump	0.8	1 mJ	50
Signal wave	1.333	~10 nJ	50

Phase matching of the I (ooe) and II (eoe) types can be implemented in the BBO crystal (oee phase matching was disregarded because of the smaller d_{eff} value). In this case the crystal must be cut at the angles θ = 19.9°, ϕ = 90° and θ = 26.2°, ϕ = 0, respectively. Type-I phase matching is characterised by a larger effective nonlinearity coefficient (1.94 pm V^{-1}) in comparison with the type-II phase matching (1.57 pm V^{-1}) [14]. However, spurious processes may occur in a BBO crystal with the I-type phase matching: second-harmonic generation (SHG) for the signal and idler waves; i.e., the nonlinear conversion processes $(1.0)^{-1}$(e) = $(2.0)^{-1}$(o) + $(2.0)^{-1}$(o) and $(0.6665)^{-1}$(e) = $(1.333)^{-1}$(o) + $(1.333)^{-1}$(o), respectively. The reason is that the phase-matching angle for the aforementioned processes is relatively close to the phase-matching angle for the main interaction (θ = 20.3° for the SHG radiation with λ_s = 1.333 μm and 21° for the SHG radiation with λ_i = 2 μm). The wave mismatch is about 8.96 cm^{-1} for the signal-wave SHG and about 15.7 cm^{-1} for the idler-wave SHG. In the BBO crystal with type-II phase matching, spurious signal-wave SHG may arise: $(0.6665)^{-1}$(e) = $(1.333)^{-1}$(o) + $(1.333)^{-1}$(o); the wave mismatch for this process is 140.79 cm^{-1}. At the same time, spurious idler-wave SHG cannot develop, because the idler wave is e-polarised.

3. Results of direct-PA simulation

We simulated the direct PA in type-I and type-II phase-matching BBO crystals pumped at λ_p = 0.8 μm, with injection of radiation at λ_s = 1.333 μm and generation of idler wave at λ_i = 2 μm. The parameters studied in the simulation were the output energies and durations (spectral widths) of signal and idler pulses in dependence of the BBO crystal length for two types of phase matching.

The following factors were taken into account when choosing the optimal crystal length. First, one must pay attention to the group velocity mismatch for the interacting pulses, which propagate through the crystal with different group velocities. The walk-off of the pulses impedes their overlap in time and thus limits the efficient conversion region. To make the influence of group velocity mismatch negligible, one must use a crystal with a length smaller than

Table 2. Characteristics of the BBO crystal and calculated values for nonlinear conversion $(0.8)^{-1} = (1.333)^{-1} + (2.0)^{-1}$ at a pump intensity of 200 GW cm^{-2}.

Phase-matching type	n_2/cm^2 W^{-1}	d_{eff}/pm V^{-1}	Phase-matching spectral width/THz	Group length L_{sp}/L_{pi} /mm	Phase-matching angle; θ/deg	Crystal length /mm
I (ooe)	2.9×10^{-16} [13]	1.94	70 (394 nm for signal wave and 933 nm for idler wave)	7.5/3	19.9	1.5
II (eoe)	2.9×10^{-16} [13]	1.57	21 (118 nm for signal wave and 280 nm for idler wave)	1.25/1.9	26.2	2

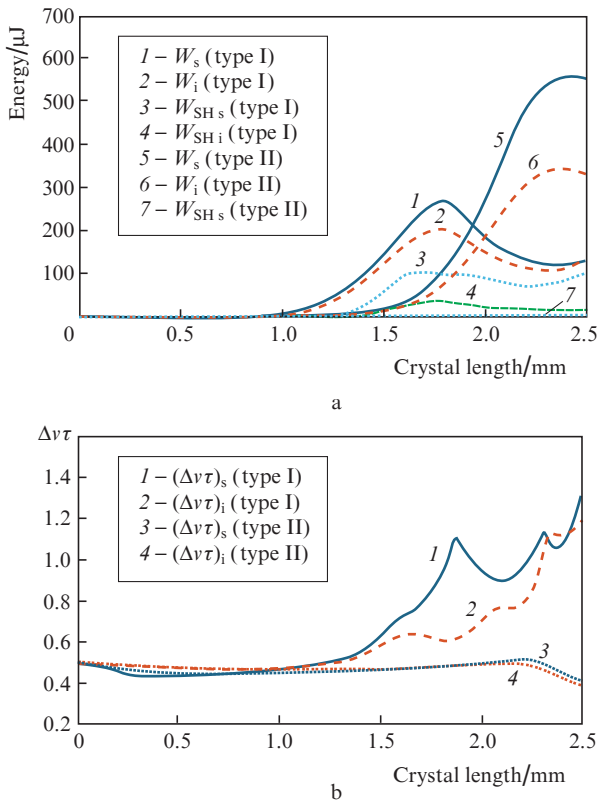

Figure 1. Dependences of the (a) energies of signal (W_s; λ_s = 1.333 μm) and idler (W_i; λ_i = 2 μm) waves and the second harmonics of signal ($W_{SH\,s}$; $\lambda_{SH\,s}$ = 0.6665 μm) and idler ($W_{SH\,i}$; $\lambda_{SH\,i}$ = 1 μm) waves and (b) the products of spectral width and pulse duration for the signal, $(\Delta v\tau)_s$, and idler, $(\Delta v\tau)_i$, waves on the crystal length.

the quasi-static interaction length (or group length); i.e., a type-I phase-matching BBO crystal less than 3 mm long or a type-II phase-matching BBO crystal less than 1.25 mm long (Table 2).

However, in the case of type-II phase-matching BBO, the efficient conversion region is not is limited by group lengths. The reason is that the group velocity mismatch for signal and pump pulses, as well as the group velocity mismatch for the idler and pump pulses have different signs. Therefore, the signal and idler pulses remain localised in the pump pulse region when propagating through the crystal, which leads to an exponential rise in gain at crystal lengths exceeding the group lengths. Figure 1 shows the dependence of the output energy on the crystal length.

Type-II phase-matching BBO crystals exhibit an increase in the signal- and idler-wave energies at crystal lengths exceeding the group lengths listed in Table 2. At a crystal length of ~2.5 mm, gain saturates, after which the output energy drops. The intensity of signal and idler waves becomes so high that the conversion is inverted: pump radiation is generated.

For the type-II phase-matching BBO crystals, the gain saturation and inverted conversion occur earlier: at crystal lengths exceeding 1.5 mm. This is related to the larger effective nonlinearity coefficient and, therefore, higher conversion efficiency. Thus, the optimal crystal length is limited by not only the group velocity mismatch but also the possibility of inverted conversion.

The optimal crystal length can also be estimated from the dependence of the product of the spectral width by the pulse duration, $\Delta v\tau$, on the crystal length (Fig. 1b). It follows from the Fourier transform properties that the product $\Delta v\tau = 0.44$ for transform-limited pulses with a Gaussian shape. In the calculations this product was estimated for each mesh spac-

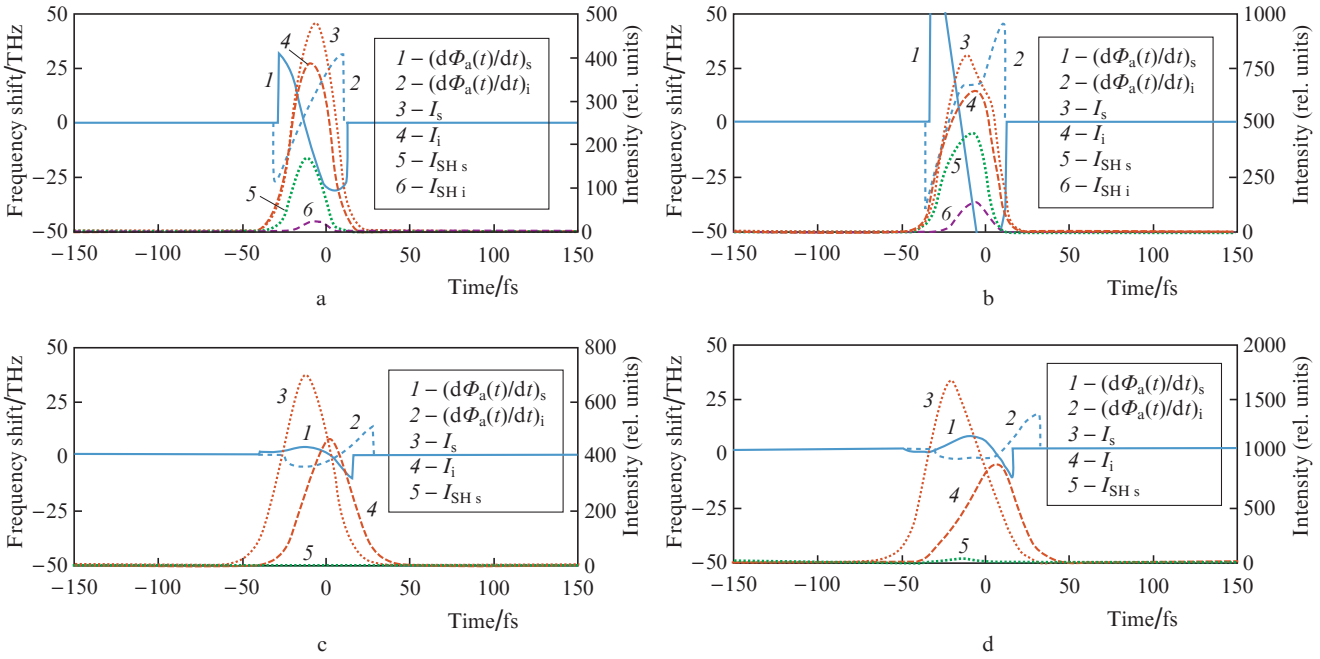

Figure 2. Temporal shapes of the pulses of signal (intensity I_s) and idler (I_i) waves, their second harmonics ($I_{SH\,s}$, $I_{SH\,i}$), and chirps $(d\Phi_a(t)/dt)_s$ and $(d\Phi_a(t)/dt)_i$ of the signal and idler waves at crystal lengths of (a) 1.5, (b) 1.7, (c) 2, and (d) 2.25 mm for the (a, b) type-I and (c, d) type-II phase matching.

ing. The values of the spectral width and duration were chosen at the half maximum of spectral and temporal distributions of pulse intensity. In the region of stable amplification of signal and idler waves, before the onset of pump depletion and at good temporal pulse overlap, the $\Delta\nu\tau$ value barely differs from 0.44 for both type-I and type-II phase matching. In the case of type-I phase matching the product $\Delta\nu\tau$ takes extremely large values (0.8–1.4) at crystal lengths above 1.5 mm, which is related to the pump pulse depletion (Figs 1b, 2a, and 2b). Similarly, a significant distortion of IR pulses is observed at crystal lengths larger than 2 mm for the type-II phase matching (Figs 1b, 2c, and 2d). Note that, at crystal lengths exceeding significantly the aforementioned values, the pulses are so distorted by inverse conversion that cannot be considered as Gaussian. In this case the $\Delta\nu\tau$ value yields no useful information.

Based on the simulation results for the type-I phase-matching BBO crystal with a length of 1.5 mm, the signal- and idler-wave energies after amplification are, respectively, 119 and 94 μJ; for the type-II phase-matching BBO crystal with a length of 2 mm, these energies are, respectively, 262 and 172 μJ. Thus, the efficiency of energy conversion into signal and idler waves for the type-II phase-matching BBO crystal is much higher ($K = 0.43$) than for the type-I phase-matching BBO crystal ($K = 0.21$), which is also demonstrated in Fig. 1a. The reason is that spurious processes (SHG for signal and idler waves) can be implemented in the type-I phase-matching BBO crystal. These processes reduce significantly the output energy of signal and idler waves and, therefore, the conversion efficiency. Efficient SHG was experimentally observed in [15]. In the type-II phase-matching BBO crystal, spurious SHG of the signal wave cannot develop at a sufficiently large wave mismatch (equal to $\sim$140 cm^{-1}) and at relatively large ($\sim$5.9°) difference in the phase-matching angles for the signal-wave SHG and the main interaction. Indeed, for the type-I phase-matching BBO crystal with a length of 1.5 mm, the second harmonic energies for the signal and idler waves are 31 and 4 μJ, respectively, whereas for the type-II phase-matching BBO crystal with a length of 2 mm, the second-harmonic energy for the signal wave is only $\sim$1 μJ (Fig. 1a).

Note that the type-I phase matching allows one to obtain larger phase-matching spectral widths (Table 2) than the type-II phase matching and, correspondingly, shorter pulses, as was confirmed by simulation. For example, the output pulse durations for the signal and idler waves were, respectively, $\sim$26 and 25 fs for the type-I phase-matching BBO crystal and 34 and 32 fs for the type-II phase-matching BBO crystal.

Thus, the use of the type-II phase-matching BBO crystal is preferred due to its higher energy conversion efficiency and the possibility of forming sufficiently short pulses: to 32 fs, which is less than five optical field cycles.

4. Results of simulating PA with chirped pump and signal wave

To increase the efficiency of converting the radiation of a Ti : sapphire laser system into the mid-IR range, with preservation of a phase-matching width sufficient for generating few-cycle pulses, a scheme of PA with a chirped signal wave and pump was considered. This scheme, in contrast to OPCPA, has more degrees of freedom, because the pump pulse remains broadband and its chirp may change independently. We performed PA simulation with chirped pulses in the type-II phase-matching BBO crystal pumped by radiation at $\lambda_p = 0.8$ μm, with radiation injection at $\lambda_s = 1.333$ μm and idler-wave generation at $\lambda_i = 2$ μm. The main purpose of this simulation was to optimise the pump and signal chirping parameters in order to obtain a maximum energy conversion efficiency and sufficiently large spectral width for signal and idler waves.

Two simulation versions were applied. In the first one the influence of the signal GDD on the energy conversion efficiency and output spectrum of signal wave with an increase in the pump pulse duration to 1 ps was determined. The pulse duration of $\sim$1 ps was chosen as a compromise to obtain a sufficient spectral width and acceptable conversion efficiency, as well as to illustrate the general trends of the change in the dependence of conversion efficiency and spectral width of signal wave on the magnitude and sign of the GDD for this wave. These trends are retained with a further increase in duration; however, the absolute values of the aforementioned parameters may change. In the second version, the signal and pump GDDs changed simultaneously, and chirping was performed to identical pulse duration.

Figure 3 shows the dependence of the energy conversion efficiency and spectral width of the signal wave on the magnitude and sign of the GDD for this wave at a fixed pump pulse GDD of 18 000 fs^2 (increase in duration to 1 ps). It can be seen that the conversion efficiency increases with an increase in the GDD of the signal pulse and is determined mainly by the temporal overlap of pump and signal pulses. When a very short signal pulse interacts with the long pump pulse, only a small part of the latter is overlapped in time with the signal pulse. This means that only a small fraction of pump energy can be converted into the signal-wave energy. A much larger amount of pump energy can be transferred to the signal pulse when the latter is sufficiently long, which is due to the better temporal overlap of pump and signal pulses propagating through the crystal and to the increase in the group interaction lengths. In particular, the highest efficiency of energy conversion into the signal wave, K_s, is obtained at identical GDDs of pump and signal pulses (to 1 ps) and amounts to $\sim$0.4, whereas the conversion efficiency into the idler wave, K_i , is $\sim$0.2. Specifically for this reason we consider below the procedure of signal and pump chirping to the identical pulse duration as the most efficient one. In addition, we should note that the conversion efficiency at chirping pump and signal pulses with identical GDD signs differs from that when the GDDs of these pulses have opposite signs. Here, a factor of key importance is the temporal overlap of spectral components during PA.

In the case where pulses with identical GDD signs are chirped, the long-wavelength spectral components of the signal wave are overlapped with the long-wavelength spectral components of the pump pulse; the central part of the signal spectrum is overlapped with the central part of the pump spectrum; and, finally, the short-wavelength components of signal wave are overlapped with the short-wavelength pump components. Thus, the phase-matching condition is satisfied for most of components of the signal pulse spectrum. In this context, chirping of pulses with identical GDD signs provides a larger spectral width and, as a conse-

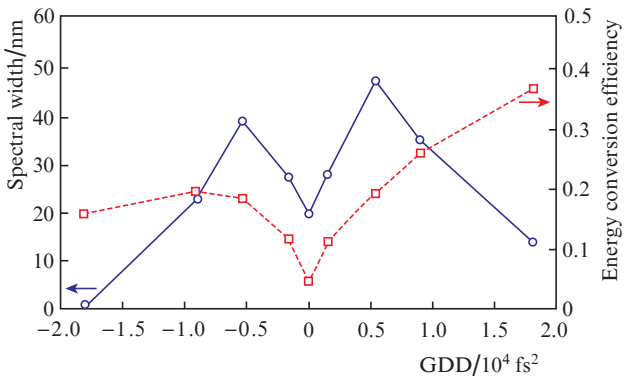

Figure 3. Dependences of the spectral width of signal pulse and energy conversion efficiency into this wave, K_s, on the GDD of signal wave at a fixed pump pulse width: 1 ps.

quence, higher energy conversion efficiency in comparison with the chirping of pump and signal pulses with different GDD signs (Fig. 3). Similarly, an increase in the energy conversion efficiency into the signal wave with an increase in the GDD for the signal pulse, as well as a possibility of implementing a higher conversion efficiency in the case of chirping signal and pump pulses with identical GDD signs, were demonstrated in [11, 16, 17]. For example, when chirping the pump (to 1 ps) and signal (to 300 fs) pulses with identical GDD signs, one can obtain the largest spectral width of ~48 nm (Fig. 3). In this case, the energy conversion efficiency into the signal wave is up to 20% (the total efficiency is up to 35%). An increase in the pump pulse width to 3 ps provided a larger spectral width (up to 58 nm) at a signal pulse duration of 500 fs; however, the conversion efficiency decreased significantly for this wave: to 12% (the total efficiency decreased to 20%).

Let us now consider the change in the spectral width of the signal pulse in the case of positive chirping signal and pump pulses. First it increases; then reaches a maximum; and, finally, decreases with an increase in the signal pulse GDD. A similar dependence of the spectral width of the signal pulse on its duration was thoroughly considered in [11, 16, 17]. For short signal pulses (with a duration of 50–100 fs), only the central part of the pump pulse interacts with the signal- and idler-wave pulses during PA. In fact, the output spectrum width is set by the group-velocity mismatch. With an increase in the signal pulse duration, the group-velocity mismatch decreases, and the output spectrum is determined by the instantaneous overlap of spectral components in the temporal representation. Then the closer the signal and pump GDD values, the wider the output spectrum. However, as can be seen in Fig. 3, the spectral width begins to decrease after a certain GDD value. This effect is explained by spectrum narrowing; it resembles a similar effect occurring in laser media (gain narrowing). Since the PA coefficient may reach values as high as 10^4, the spectral components falling in the pump pulse tails are amplified much more weakly than the components at the pulse centre. Thus, a maximum arises in the dependence on the spectral width of the signal pulse on the GDD value. In this context, when developing a double chirped parametric amplifier, one must choose between the maximum conversion efficiency and maximum spectral width.

Since identical GDD values for pump and signal pulses provide a maximum energy conversion efficiency, we will consider now a change in the absolute GDD values for both waves simultaneously in order to determine the possibilities of increasing the spectral width of the signal pulse. In this case the simulation was aimed at studying the dependence of the spectral width of idler pulse on the magnitude and sign of GDD for the pump and signal pulses. The parameters used in the simulation are listed in Table 3. The pump intensity at the BBO crystal input was taken to be ~200 GW cm^{-2}.

Table 3. Parameters of signal and pump pulses.

Radiation	Wavelength /μm	GDD /fs^2	Pulse duration	Energy
Pump	0.8	0–90000	50 fs – 5 ps	1 mJ
Signal wave	1.333	from –90000 to +90000	50 fs – 5 ps	10 nJ

Figure 4 shows the spectra of signal (1.333 μm) and idler (2 μm) waves as functions of the GDD value and sign for the pump and signal pulses. It can be seen that the spectral width of the signal pulse remains practically the same at all GDD values. In contrast, the idler pulses exhibit the narrowest spectrum (to 10–13 nm) when the signal and pump pulses are chirped with identical signs, and a much more wider spectrum (to 100 nm) in the case of chirping with different GDD signs. This is related to the fulfilment of 'instantaneous' phase-matching conditions. When chirping with identical GDD signs, the difference in the frequencies of pump and signal waves, whose pulses are temporarily overlapped, is small. The GDD values for the pump and signal pulses are almost compensated for during generation of idler pulse, and the latter turns out to be non-chirped and have a fairly narrow spectrum. When the signs of GDDs for pump and signal pulses are opposite (positive and negative, respectively), the long-wavelength components of signal pulse are overlapped with the short-wavelength components of the pump pulse in the temporal representation. Therefore, the signal at the difference frequency of pump and signal pulses (idler pulse) has the largest spectral width, due to which pulses can be compressed to a duration of ~59 fs. A similar dependence of the spectral width of idler pulses on the sign of GDDs of signal and pump pulses was also demonstrated in [16, 17].

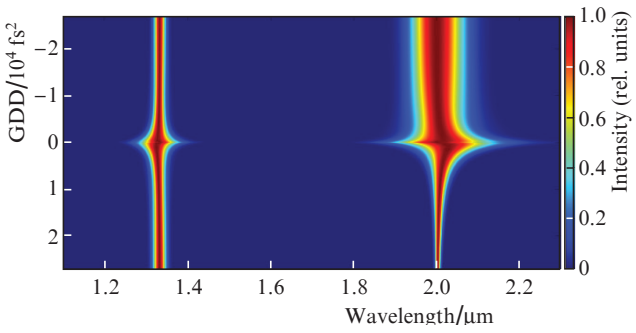

Figure 4. (Colour online) Spectra of signal and idler pulses as functions of the GDD of these pulses.

Note that Fu et al. [16] could obtain the widest signal-wave spectrum when chirping signal and pump pulses with identical GDD signs, which was explained by a more exact fulfilment of the phase-matching condition. In our study the spectral width of signal pulse is also larger in the case of chirping with identical GDD signs (~23 nm); however, its difference from the case of chirping with different GDD signs (~20 nm) is small. To explain this behaviour of the signal spectral width, we investigated its dependence on the initial pump pulse width τ_0 at a fixed GDD value for this pulse: ~18000 fs^2, because, in contrast to [16], we used radiation of a Ti:sapphire laser with τ_0 = 50 fs. The τ_0 value was varied from 25 to 100 fs in the simulation (the pump pulse width in [16] was ~25 fs). Figure 5 demonstrates a significant increase in the spectral width of the signal pulse under identical chirping conditions, in dependence of the initial pump pulse width. In particular, at τ_0 = 25 fs one can obtain a larger spectral width of signal wave (up to 46 nm) than at τ_0 = 50 fs. In this case, the conversion efficiency into the signal wave is up to 30%, and the total conversion efficiency is up to 50%. Thus, the spectral width of the initial pump pulse decisively affects the possibility of generating a broadband signal pulse. For pump pulses with a moderate spectral width, the most broadband signal pulse can be obtained only in the direct-amplification scheme, whereas the use of double chirping leads either to a narrowing of the signal wave spectrum or a decrease in the conversion efficiency.

Thus, proceeding from our consideration, the most promising approach is direct amplification in a 2-mm-long type-II phase-matching BBO crystal. In this case, to implement the last conversion cascade at an energy of ~50 mJ, the beam size must be ~2.5 cm. To date, crystals with an aperture of 10 × 10 mm are commercially available. In addition, a faceted crystal, which was applied previously to generate THz radiation [18], can also be used. According to our calculations, this crystal can provide a signal wave energy up to 10 mJ and an idler wave energy up to 6.2 mJ, with preservation of pulse durations at levels of 33 and 36 fs, respectively. Note that the pump intensity, as well as the crystal length in the output cascades, must be optimised to preserve the pump pulse duration and exclude pump depletion.

5. Conclusions

We performed a numerical simulation of the schemes of direct PA and PA with chirped signal and pump pulses in type-I (ooe) and type-II (eoe) phase-matching BBO crystals. The pump source was a terawatt Ti:sapphire laser (λ_p = 0.8 μm, τ = 50 fs, W = 60 mJ). It was shown that, for the type-I phase-matching BBO crystal with a length of 1.5 mm, the energy conversion efficiency into signal and idler waves is fairly low (21%) because of the high conversion efficiency into the spurious second harmonics of signal and idler waves. However, the durations of signal (λ_s = 1.333 μm) and idler (λ_i = 2 μm) pulses amount up to 26 fs, which is due to the large phase-matching spectral width (394 and 933 nm for the signal and idler waves, respectively). For the type-II phase-matching BBO crystal with a length of 2 mm, the energy conversion efficiency is much higher (43%) because of the absence of spurious processes (SHG for the signal and idler waves), despite the smaller effective nonlinearity coefficient (d_{eff} = 1.57 pm V^{-1}) in comparison with that for type-I phase matching (d_{eff} = 1.94 pm V^{-1}). The output durations of signal and idler pulses are 34 and 32 fs, respectively.

The consideration of the double chirping scheme showed that the total energy conversion efficiency into signal and idler waves can be increased to 60% by chirping signal and pump pulses to a duration of 1 ps, which is related to the better temporal overlap of pump and signal pulses during their propagation through the crystal. However, the spectral width of the signal pulse in this case is only 23 nm, which corresponds to its duration of 108 fs. The spectral width cannot be increased by changing the GDD value with preservation of conversion efficiency. A signal-wave spectral width of 48 nm can be obtained at a conversion efficiency of about 20% by chirping the signal pulse to a duration of 300 fs and the pump pulse to 1 ps; in this case, the total conversion efficiency may reach 35%. A much larger width of the output spectrum (up to 46 nm) can also be obtained for shorter (25 fs) pump pulses at an energy conversion efficiency into the signal wave up to 30% (with the total energy conversion efficiency reaching 50%). Note that the maximum spectral width of the idler pulse (to 100 nm) is obtained by chirping the signal and pump pulses with opposite GDD signs, due to which idler pulses can be further compressed to ~65 fs.

Thus, when using 50-fs pump pulses, the direct-amplification scheme is preferred because of its higher efficiency and possibility of generating short pulses.

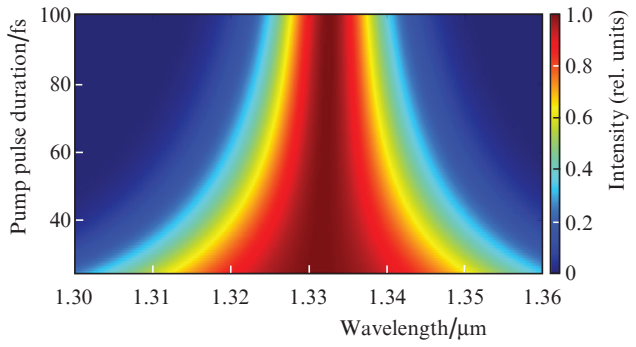

Figure 5. (Colour online) Spectrum of the signal wave pulse as a function of the initial pump pulse width.

Acknowledgements. This work was supported by the Russian Science Foundation (Project No. 20-19-00148).

References

1. Vicario C., Ovchinnikov A.V., Ashitkov S.I., Agranat M.B., Fortov V.E., Hauri C.P. *Opt. Lett.*, **39** (23), 6632 (2014).
2. Jazbinsek M., Puc U., Abina A., Zidansek A. *Appl. Sci.*, **9** (5), 882 (2019).
3. Fedorov V.Y., Tzortzakis S. *Opt. Express*, **26** (24), 31150 (2018).
4. Vasilyev S., Moskalev I., Mirov M., et al. *Proc. SPIE*, **10193**, 101930U (2017).
5. Migal E., Pushkin A., Bravy B., Gordienko V., Minaev N., Sirotkin A., Potemkin F. *Opt. Lett.*, **44** (10), 2550 (2019).
6. Danson C.N., Haefner C., Bromage J., et al. *High Power Laser Sci. Eng.*, **7**, e54 (2019).
7. Fu Y., Xue B., Midorikawa K., Takahashi E.J. *Appl. Phys. Lett.*, **112** (24), 241105 (2018).
8. Xu L., Nishimura K., Suda A., Midorikawa K., Fu Y., Takahashi E.J. *Opt. Express*, **28** (10), 15138 (2020).

9. Takahashi E.J., Kanai T., Nabekawa Y., Midorikawa K. *Appl. Phys. Lett*., **93** (4), 041111 (2008).
10. Vaupel A., Bodnar N., Webb B., Shah L., Richardson M.C. *Opt. Eng*., **53** (5), 051507 (2013).
11. Zhang Q., Takahashi E.J., Mücke O.D., Lu P., Midorikawa K. *Opt. Express*, **19** (8), 7190 (2011).
12. Zhang D., Kong Y., Zhang J.Y. *Opt. Commun*., **184** (5-6), 485 (2000).
13. Koechner W. *Solid-state Laser Engineering* (Berlin – Heidelberg: Springer, 2013) Vol. 1.
14. Eckardt R.C., Masuda H., Fan Y.X., Byer R.L. *IEEE J. Quantum Electron*., **26** (5), 922 (1990).
15. Xu G., Wandel S.F., Jovanovic I. *Rev. Sci. Instrum*., **85** (2), 023102 (2014).
16. Fu Y., Midorikawa K., Takahashi E.J. *Sci. Rep.*, **8** (1), 1 (2018).
17. Fu Y., Midorikawa K., Takahashi E.J. *IEEE J. Sel. Top. Quantum Electron*., **25** (4), 1 (2019).
18. Vicario C., Shalaby M., Hauri C.P. *Phys. Rev. Lett*., **118** (8), 083901 (2017).